THE EUROPEAN
PHYSICAL JOURNAL C

Event-shape engineering analysis of D meson in ultrarelativistic heavy-ion collisions

Maria Lucia Sambataro[1,2], Yifeng Sun[3,1,2], Vincenzo Minissale[1,2] , Salvatore Plumari[1,2,a], Vincenzo Greco [1,2]

[1] Department of Physics and Astronomy "E. Majorana", University of Catania, Via S. Sofia 64, I-95123 Catania, Italy

[2] Laboratori Nazionali del Sud, INFN-LNS, Via S. Sofia 62, I-95123 Catania, Italy

[3] School of Physics and Astronomy, Shanghai Key Laboratory for Particle Physics and Cosmology, and Key Laboratory for Particle Astrophysics and Cosmology (MOE), Shanghai Jiao Tong University, Shanghai 200240, China

Abstract We describe the propagation of charm quarks in the quark-gluon plasma (QGP) by means of an event-by-event transport approach. In our calculations the non-perturbative interaction between heavy quarks and light partons has been taken into account through a quasi-particle approach with thermal light quark masses tuned to reproduce lQCD thermodynamics. We found that the flow observables v_2 and v_3 of D mesons are comparable with the experimental measurements for Pb + Pb collisions at 5.02 TeV in different ranges of centrality selections. The results are analyzed with event-shape engineering technique. The comparison of the anisotropic flow coefficients v_n with experimental data show a quite good agreement with experimental data for different flow vector q_2 selections, which confirms the strong coupling between charm quarks and light quarks in the QCD matter. Furthermore, we present here a novel study of the event-by-event correlations between flow harmonics of D mesons and soft hadrons at LHC energy with the event-shape engineering technique that can put further constraints on heavy quark transport coefficients toward a solid comparison between the phenomenological determination and the lattice QCD calculations.

1 Introduction

Heavy quarks (HQs), mainly charm and bottom quarks, are produced in the early stages of a ultra-relativistic heavy-ion collision (uRHIC) by hard processes described by perturbative QCD calculations. They have been identified as one among the few probes which may allow for a direct study of the QGP properties. This is manly due to the following rea-

sons related to their large masses: (i) they have a very short formation time ($\tau \sim 0.1$ fm/c), (ii) HQs are not expected to reach a full thermalization. Therefore, they can probe the entire space-time evolution of the matter created in these collisions. Furthermore, due to their interaction with the medium produced (quarks and gluons) they can keep this information in their final state as constituent of heavy hadrons mainly D, B mesons and Λ_c, Λ_b baryons. Among the several observables studied in uRHICs two of them have been long investigated for HF hadrons: the heavy mesons nuclear modification factor $R_{AA}(p_T)$ [1–3], and the so called elliptic flow, $v_2(p_T)$. The first gives an information about the change of the spectrum in AA collision with respect to a simple pp superposition. The second gives a measure of the anisotropy in the particle angular distribution and allows to investigate the coupling of the HQs with the medium and their participation in the collective motion. Both these quantity have been extensively used as probe of the Quark Gluon Plasma [4,5]. From a theoretical point of view, in recent years, several studies have done efforts in the direction of studying both of these observables to understand the heavy quark dynamics in QGP [6–22].

More recent measurements on the D mesons and Λ_c production in nuclear collisions unfolded the possibility to get access to richer information. In particular, some studies have opened the way to address the issue of medium-modification of heavy-flavour hadronization making possible to get information about the hadronization process and possibly validate models based on the recombination [23]. Recently these studies have been extended to the case of small collision systems like proton–nucleus and proton–proton collision providing insight on the heavy flavor hadronization mechanism and the possibility that also in such small systems the QGP can be formed [24].

[a] e-mail: salvatore.plumari@dfa.unict.it (corresponding author)

Springer

More information about the interactions of heavy quarks with the medium can be obtained through measurements of the azimuthal distributions of heavy-flavour hadrons produced in a HIC. Because of the interaction of heavy quarks with the medium, the spatial anisotropy in the early stages of nucleus-nucleus collisions is converted into an azimuthally anisotropic distribution in momentum space for the final particles produced from the QGP. The anisotropy is characterised in terms of the Fourier coefficients v_n of the final distribution respect to the symmetry-plane angles Ψ_n (for the harmonic of order n). The second coefficient of this expansion is the elliptic flow v_2 which is the dominant contribution in non-central collisions. The higher order harmonics usually studied are the triangular flow v_3, and the v_4; the measurement of odd harmonics of heavy-flavour hadrons or their event-by-event fluctuations coming from the random nucleon positions can provide a richer information on the initial conditions. Recently, the triangular flow v_3 has been investigated in studies based on Langevin or Boltzmann approaches on an event-by-event analysis [25–29]. One of the new tools that can be used to further investigate the dynamics of heavy quarks in the medium is the Event-Shape-Engineering (ESE) technique [30]. This technique enables to select events in heavy-ion collisions characterized by an high or low eccentricity, furnishing the chance to study the system evolution dynamics and the role of the initial conditions. This technique was first used by the ALICE Collaboration in the light-flavour sector to study the interplay between the initial geometry of the nucleus-nucleus collisions and the subsequent evolution of the system [31] and recently it was extended to investigate the sensitivity of the D meson v_2 to the event-shape selection [32]. These measurements have shown a sizeable sensitiveness to the event-shape selection, confirming a correlation between the D-meson azimuthal anisotropy and the underlying collective expansion of the bulk matter. In this paper we use an event-by-event transport approach for the evolution of heavy quarks and we study the correlation of heavy-quark anisotropic flows $v_n - v_m$ performing an analysis with the ESE technique.

The paper is organized as follows. In Sect. 2 we briefly discuss the Boltzmann transport approach used to describe the HQs evolution and the hadronization model used, furthermore we will describe the initial conditions employed in the simulation. In Sect. 3 we discuss the comparison between the simulation results and the experimental data for the anisotropic flows coefficients v_n at different centralities. In Sect. 4 we introduce the ESE technique and we show and discuss the outcome for the anisotropic flows coefficients and their correlations. Finally, Sect. 5 contains a summary and some concluding remarks.

2 Heavy quarks transport approach

We use a transport code developed to perform studies of the dynamics of relativistic heavy-ion collisions at both RHIC and LHC energies [33–43]. The space-time evolution of gluons and light quarks as well as of charm quarks distribution functions is described by mean of the relativistic Boltzmann transport (RBT) equations given by

$$p_q^\mu \partial_\mu f_q(x, p) = \mathcal{C}[f_q, f_g](x_q, p_q) \tag{1}$$

$$p_g^\mu \partial_\mu f_g(x, p) = \mathcal{C}[f_q, f_g](x_g, p_g) \tag{2}$$

$$p^\mu \partial_\mu f_Q(x, p) = \mathcal{C}[f_q, f_g, f_Q](x, p) \tag{3}$$

where $f_i(x, p)$ is the on-shell phase space one-body distribution function for i-th parton species and in the right-hand side $\mathcal{C}[f_q, f_g, f_Q](x, p)$ is the relativistic Boltzmann-like collision integral accounting for $2 \to 2$ scattering processes. For the distribution functions of the quarks and gluons that compose the QGP medium, the evolution is described by Eqs. (1) and (2) in this paper. We assume that these Eqs. are independent of f_Q, which correspond to discard collisions between charm quarks and the bulk in the determination of light quarks and gluons distribution functions, which is by far a solid approximation. In both collision integrals the total cross section is determined in order to keep the ratio $\eta/s = 1/(4\pi)$ fixed during the evolution of the QGP, see Refs. [36,40,42,44] for more details. Furthermore, in the present paper we have employed a bulk with thermal massive quarks and gluons according to a quasi-particle model (QPM) such that the system has approximately the lattice QCD equation of state, with a softening of the equation of state consistent with a decreasing speed of sound approaching the crossover region [45]. For the heavy quark interacting with the bulk medium we consider a QPM whose main feature is that the resulting coupling is significantly stronger than the one coming from pQCD running coupling, particularly as $T \to T_c$ (see details in Refs. [17,41]). Numerically we solve the RBT equation using the test particle method, where the collision integral is solved by Monte Carlo method based on stochastic interpretation of transition amplitude [33,46,47]. In our calculations the viscosity is fixed by determining the total isotropic cross section according to the Chapman–Enskog approximation:

$$\eta = f(z)\frac{T}{\sigma} \tag{4}$$

where $z = m/T$ while the function $f(z)$ is defined by the following expression

$$f(z) = \frac{15}{16} \frac{\left(z^2 K_3(z)\right)^2}{(15z^2 + 2)K_2(2z) + (3z^3 + 49z)K_3(2z)} \tag{5}$$

where $K_n(z)$ are the modified Bessel functions. As shown in Ref. [33] the above expression for the shear viscosity η is in quite good agreement with the Green–Kubo formula.

At the end of the evolution at freeze-out temperature, we use the hybrid hadronization approach via coalescence plus fragmentation as shown in Refs. [23].

In our simulation for parton initial conditions, we have employed a modified Monte Carlo Glauber model, used in [43] and inspired by wounded quark model. In this model each nucleon is composed by three constituent quarks that are randomly distributed within each nucleon according to the distribution $dN/dr = \frac{r^2}{r_0^3}e^{-r/r_0}$ with $r_0 = 0.3$ fm and the final center of mass of the three quarks is translated to the position of the nucleon, which corresponds to a proton charge RMS value of 0.84 fm. The positions of nucleons in Pb nuclei are instead distributed according to the standard Woods–Saxon distribution. In this way we generate the wounded quark profile using Monte-Carlo Glauber model and we decide whether each quark pair from target and projectile can collide or not with a probability $p = e^{-\pi r^2}/\sigma_{qq}$ with $\sigma_{qq} = 13.6$ mb in 5.02 TeV $Pb + Pb$ collision [48]. This procedure leads to an inelastic nucleon–nucleon cross section of 70.3 mb at 5.02 TeV collisions.

Finally, the total initial parton distribution is given by:

$$\frac{dN}{d^2\mathbf{x}_\perp d\eta} = \sum_{i=1}^{N_{part}} n_i \rho_\perp(\mathbf{x}_\perp - \mathbf{x}_i)\rho(\eta) \qquad (6)$$

where N_{part} is the number of participant quarks while $\mathbf{x}_i$ and n_i are the transverse position of each participant quark and the parameter that controls the contribution of the i-th wounded quark to particle production respectively. The profile in the transverse position $\rho_\perp(\mathbf{x}_\perp)$ is expressed as follows:

$$\rho_\perp(\mathbf{x}_\perp) = \frac{1}{2\pi\sigma^2}e^{-\frac{\mathbf{x}_\perp^2}{2\sigma^2}}. \qquad (7)$$

While the profile for the distribution of the spatial rapidity $\rho(\eta)$ is given by longitudinal boost invariance in pseudo-rapidity. In Eq. 6 the numbers n_i fix the number of partons produced in each event. This number is given by $n_0 N$ where N is sampled according to a negative binomial distribution given by

$$P(N) = \frac{\Gamma(N+k)\bar{n}^N k^k}{\Gamma(k)N!(\bar{n}+k)^{N+k}} \qquad (8)$$

where n_0 is fixed in order to have that the final charged particle multiplicity is same as that measured in experiments. This model is inspired by the distribution of the number of particles produced in pp collisions that fluctuates according to a negative binomial distribution. In order to reproduce the distribution of charged particles measured by ALICE Collaboration the parameters have been fixed to $k = 0.224$, $\bar{n} = 1.621$ and $n_0 \approx 1.88$.

In momentum space we have considered a mixture of a *soft* and an *hard* component, with the former consisting of quarks and gluons with an initial thermal equilibrium distribution, and the latter being equivalent to the products of initial binary pQCD collision consisting of 'minijets'. The soft partons are distributed according to the following

$$\frac{dN}{d^2\mathbf{x}_\perp d\eta} = \frac{g\tau_0}{(2\pi)^2}p_T m_T \qquad (9)$$

$$\times \cosh(\eta - y)\exp\left(-\frac{m_T \cosh(\eta - y)}{T(\mathbf{x}_\perp, \eta)}\right)dp_T dy$$

$$(10)$$

where $g = 2 \times 8 + 3 \times 2 \times 6 = 52$ is the degree of freedom of partons (three flavor quarks and gluons), $\tau_0 = 0.4$ fm/c is the termalization time and $m_T = \sqrt{m^2 + p_T^2}$ is the transverse mass of light partons. The transverse momentum distributions of minijets at mid-rapidity are taken from pQCD calculations and we have used the spectra of gluons and quarks from CUJET Collaboration [49] for pp collisions at 5.02 TeV.

In coordinate space we initialize the charm quark distribution in accordance with the number of binary nucleon–nucleon collisions, N_{coll}, from the Monte Carlo Glauber model. Finally, for the charm quark initial distribution in momentum space we use the production calculated at Fixed Order + Next-to-Leading Log (FONLL) [50] which describes the D-meson spectra in proton-proton collisions after fragmentation. For detail we refer to our earlier work in Ref. [41].

In our simulation when the temperature of the QGP phase goes below the quark-hadron transition temperature, $T_c = 155$ MeV, the light and heavy quarks can hadronize. For the heavy quark hadronization process, we consider a hybrid approach of hadronization by coalescence plus fragmentation. The fragmentation is implemented using the Peterson fragmentation function [51]: $f(z) \propto [z[1 - \frac{1}{z} - \frac{\epsilon_c}{1-z}]^2]^{-1}$ where $z = p_D/p_c$ is the momentum fraction of the D-meson fragmented from the charm quark and ϵ_c is a free parameter to fix so that one can describe D-meson production in proton-proton collisions [52]. For the coalescence model, it is based on a Wigner formalism. In our calculation the Wigner function is assumed to be Gaussian where the widths are fixed by the mean square charged radius of the D meson, for detail we refer to our earlier work [23]. In the light sector, we consider charged particles that come from an hadronization via coalescence plus fragmentation, as in Ref. [53].

3 Heavy flavour anisotropic flows $v_n(p_T)$

In a non-central nucleus-nucleus collision, the interaction of the QGP constituents, convert the initial eccentricity of the
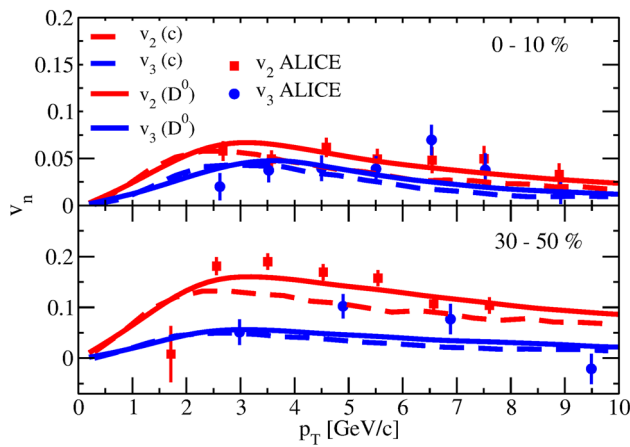
Fig. 1 v_2 and v_3 of charms quarks (dashed lines) and D mesons (solid lines) as a function of p_T at mid-rapidity and for centrality classes $0-10\%$ (upper panel) and $30-50\%$ (lower panel) for $PbPb$ collisions at 5.02 TeV. Data are taken from ALICE measurements [56]

overlap region into a final anisotropy in momentum space, characterised in terms of the Fourier coefficients $v_n(p_T)$.

In our model, event-by-event fluctuations generate a profile in the transverse plane $\rho_\perp(\mathbf{x}_\perp)$ that change with the event and which determines in each event the initial anisotropy in coordinate space. This is quantified in terms of different order spatial asymmetries named ϵ_n and expressed by:

$$\epsilon_n = \frac{r_\perp^n \cos[n(\phi - \Psi_n)]}{r_\perp^n} \tag{11}$$

$$\Psi_n = \frac{1}{n} \arctan \frac{r_\perp^n \sin(n\phi)}{r_\perp^n \cos(n\phi)} \tag{12}$$

where $r_\perp = \sqrt{x^2 + y^2}$ and $\phi = \arctan(y/x)$.

The results shown in this paper have been obtained using the two particle correlation method to calculate elliptic (v_2) and triangular flow (v_3) and v_4 [54,55]. We have found that the number of test particles $N_{\text{test}} \sim 350$ and the lattice discretization $\Delta x = \Delta y = 0.3$ fm in the simulations guarantee a convergence for $v_{2,3}(p_T)$ up to $p_T \sim 8$ GeV/c.

In Fig. 1, we show the D mesons anisotropic flow coefficients $v_2(p_T)$ and $v_3(p_T)$ at mid-rapidity for $Pb + Pb$ collisions at 5.02 TeV for central (0–10%) in the upper panel and semi-peripheral (30–50%) collisions in the bottom panel, where the centrality class is selected based on the charged-particle multiplicity.

The red line corresponds to $v_2(p_T)$ and blue line to $v_3(p_T)$ both for charm quarks (dashed line) and D mesons(solid line). The charm quarks v_2 and v_3 are different from zero in both centrality classes suggesting that charm quarks take part in the collective motion. We observe that the v_2 is sensitive to the centrality of the collisions while the v_3 has a weak dependence with the centrality and it is comparable for both centralities. This suggests that the elliptic flow is mainly gen-

erated by the geometry of overlapping region and it is larger for larger centrality collision while triangular flow is mainly driven by the fluctuation of the triangularity ϵ_3 of overlapping region , and similar results observed also for light quarks [40,57]. The hadronization mechanism plays a role for the v_2 to describe D meson anisotropic flow at intermediate p_T range. The effect of coalescence corresponds to an increase of the collective flows at $p_T > 2$ GeV due to the fact that D mesons are formed by the recombination of a light and a heavy quarks. This effect is mainly due to the elliptic flow of light quarks which is larger than the one of charm quarks. The process of the couple recombination gives as a result a final hadron elliptic flow larger respect to the simple anisotropy of the initial charm, because it carries information from both quarks anisotropies. On the other hand, D mesons coming from fragmentation have always a smaller momentum with respect to the original charm quark, as a result the fragmentation contribution to the elliptic flow is similar to the one at charm level but shifted to lower p_T. As shown in Fig. 1, our results are in good agreement with the ALICE experimental data [56] and capture the centrality dependence observed experimentally.

4 Event-shape engineering technique

Further investigation into the dynamics of heavy quarks in the medium can be performed with the event-shape engineering (ESE) technique [30]. This technique is based on the observation that the event-by-event variation of the anisotropic flow coefficient v_n at fixed centrality is very large [58]. This technique allows for selection of events with the same centrality but different initial geometry on the basis of the magnitude of the average bulk flow q_2. In this section, we present the main features of the ESE selection and our results with this approach focusing on the prediction for anisotropic flows correlations $v_n - v_m$ in the heavy flavor sector. In order to apply the ESE technique, in our calculations the events in each centrality class are divided according to the magnitude of the second-order harmonic reduced flow vector q_2 which is defined as:

$$q_2 = \frac{|\mathbf{Q}_2|}{\sqrt{M}} \tag{13}$$

where $\mathbf{Q}_2$ is a vector built from the azimuthal angles ϕ_k of the considered particles and given by

$$\mathbf{Q}_2 = \sum_{k=1}^{M} e^{i2\phi_k} \tag{14}$$

while M is the number of charged particles in the specific range of transverse momentum p_T and pseudorapidity η.
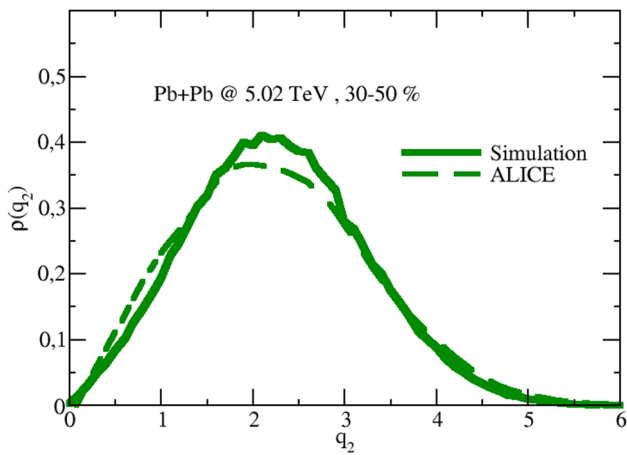
Fig. 2 Distribution of charged particles at mid-rapidity ($|\eta| < 0.8$) as a function of the reduced flow vector q_2. In the transverse momentum range $0.2 < p_T < 5$ GeV/c for the $30 - 50\%$ centrality class in 5.02 TeV $PbPb$ collisions, compared to the ALICE measurements taken from [59]

In Fig. 2, it is shown q_2 distribution of charged particles with $|\eta| < 0.8$ and in the transverse momentum range $0.2 < p_T < 5$ GeV/c for 30–50% centrality class in $PbPb$ collisions at 5.02 TeV. The selection of the events according to the average bulk flow q_2 was performed by using q_2 percentiles in 1%-wide centrality intervals to make our results comparable with the experimental data [56].

Our results shown by the solid line are in in good agreement with the ALICE measurements [59] (dashed line). This kind of study can be performed with the implementation of event-by-event initial state fluctuations, and we are performing one of the first calculation of this type concerning the dynamics of heavy quark.

A first study on the heavy-light flavor correlations of anisotropic flows at LHC energies with an event-by-event transport approach has been performed by means of a full Boltzmann transport approach in Ref. [29]. In this paper we extend that work and evaluate the correlations between different order anisotropic flows $v_n - v_m$ both in the light and heavy flavor sectors with the ESE technique.

In Fig. 3, we have shown different spatial bulk eccentricities ϵ_n as a function of reduced flow vector q_2 for $Pb + Pb$ collisions at $\sqrt{s_{NN}} = 2.76$ TeV in 30–50% centrality class. The results show that large q_2 corresponds to events where the fireball has a large initial eccentricity ϵ_2. The triangularity ϵ_3 show a weak anti-correlation while ϵ_4 receives a non linear contribution with respect to q_2. The correlation between the spatial eccentricities ϵ_n-ϵ_m that is present in the initial geometry gives rise to correlation between different flow harmonics v_n-v_m.

Hydrodynamic and transport calculations have shown that the response of the system to the initial spatial anisotropy is essentially linear for the second and third harmonics, mean-
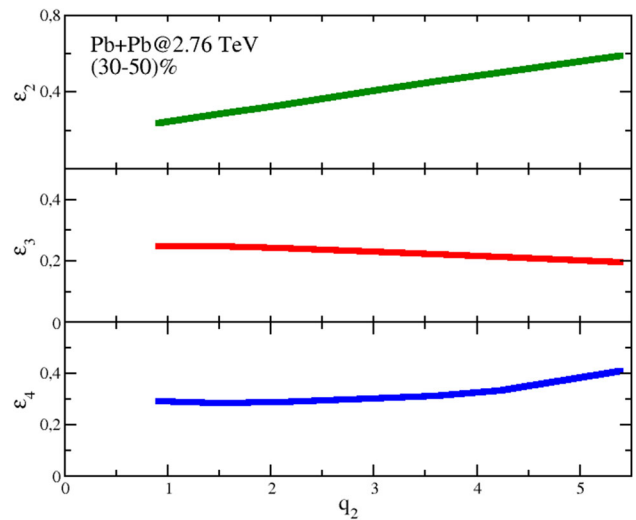

Fig. 3 Different order spatial eccentricities $\epsilon_{n=2,3,4}$ as a function of reduced flow vector q_2 for $\sqrt{s_{NN}} = 2.76$ TeV $PbPb$ collisions
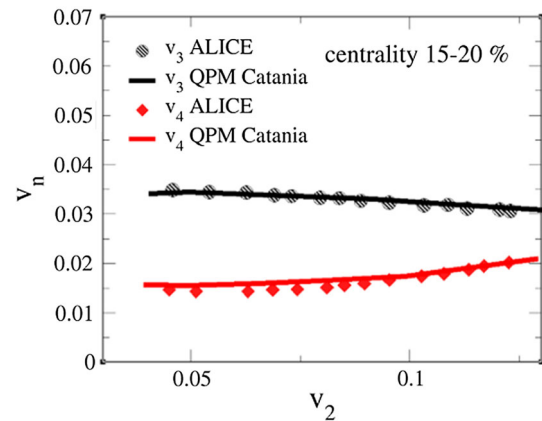
Fig. 4 Correlations between v_n and v_m ($n = 2, m = 3, 4$) for charged particles in $PbPb$ collisions at $\sqrt{s_{NN}} = 2.76$ TeV for $15 - 20\%$ centrality class. The red and black points are experimental data taken from ALICE Collaboration [63]

ing that the final state v_2 and v_3 are very well correlated with the second and third order eccentricities in the initial state, for small values of η/s [40,60–62]. In Fig. 4 the correlations between v_2 and v_3 (solid black line), v_2 and v_4 (red solid line) for charged particles in $PbPb$ collisions at $\sqrt{s_{NN}} = 2.76$ TeV in 15–20% centrality class are shown in comparison with the experimental data from ALICE Collaboration [63]. In these calculations, for a given centrality class, every point is determined evaluating the v_n varying the q_2. The trend of the $v_n - v_2$ correlations is related to the initial correlation (anti-correlation) between ϵ_n and ϵ_2, because of the strong linear correlations for each harmonic $v_n \propto \epsilon_n$. The initial anti-correlation between the ϵ_2 and ϵ_3 can be understood considering, for example, that having, for a determined centrality, a specific number of participating nucleons can be ideally arranged to have a large ϵ_2, the geometric con-
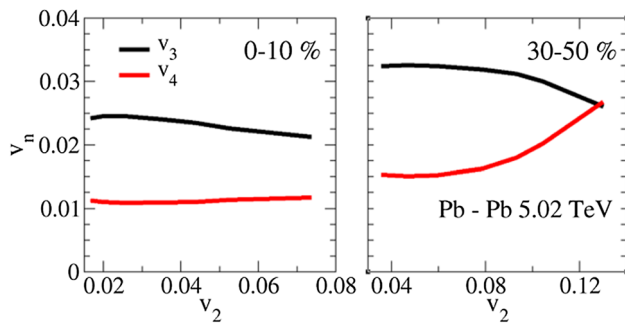
Fig. 5 v_n and v_m ($n = 2, m = 3, 4$) correlations for D mesons in $PbPb$ collisions at $\sqrt{s_{NN}} = 5.02$ TeV for both 0–0% (left panel) and 30-50% (right panel) centrality class


Fig. 6 Symmetric cumulant correlator $SC(m, n)$ for both charged particles (left panel) and prediction for D mesons (right panel) as a function of centrality class. In the left panel the experimental data taken from ALICE Collaboration [68]

sequence of this configuration leads to a smaller ϵ_3. These results are in agreement with other measurement performed by the ATLAS Collaboration [64]. As shown in Fig. 4 the v_4 has a non linear correlation with the v_2. This behaviour can be attributed to the fact that v_4 receives a non-linear contribution from the initial ϵ_2 that goes like $(\epsilon_2)^2$ [57]. On the other hand, the v_4 can be parametrized as the quadrature sum of two components: one proportional to v_2^2 (as $v_2 \propto \epsilon_2$) that comes from the non-linear hydrodynamics response of the medium, and the other contribution that in principle could be a linear component that should be independent of v_2 [65,66]. Our results for charged particles are in good agreement with the experimental data suggesting that our approach may capture the initial spatial fluctuations of the bulk matter. In the same scheme in Fig. 5 we have evaluated the v_n-v_m correlations in the charm sector giving predictions for v_2-v_3 and v_2-v_4 for D mesons in $PbPb$ collisions at $\sqrt{s_{NN}} = 5.02$ TeV in most central 0–0% and semi-peripheral 30–50% centrality classes. As for the light quark sector, we can clearly see an anti-correlation between v_2-v_3 and a non linear, quadratic correlation between v_2-v_4. We observe a weak correlation between $v_3 - v_2$ and $v_4 - v_2$ in the central collisions and the correlation (or anti-correlation) becomes larger in more peripheral collisions. Moreover, as shown in [29] the correlation coefficient between the heavy and light quarks v_2 is about $C \approx 0.95$ and it remains almost flat and independent of impact parameter, suggesting a very strong correlation between the final charm quark v_2 and light quark v_2 for all the centrality investigated. On the other hand, it was approximately observed the same degree of correlation for v_2, v_3 and v_4. This suggest that the building up of v_n of heavy quarks is driven by the v_n of the bulk for $n = 2, 3, 4$. This can explain why we predict a similar $v_n - v_m$ correlations of heavy quarks like the ones of the bulk.

In order to perform a more systematic study we can now introduce a new type of observable for anisotropic flow analyses, the so-called *Symmetric Cumulant* ($SC(m, n)$), proposed in [67]. This observable is particularly useful for systems in
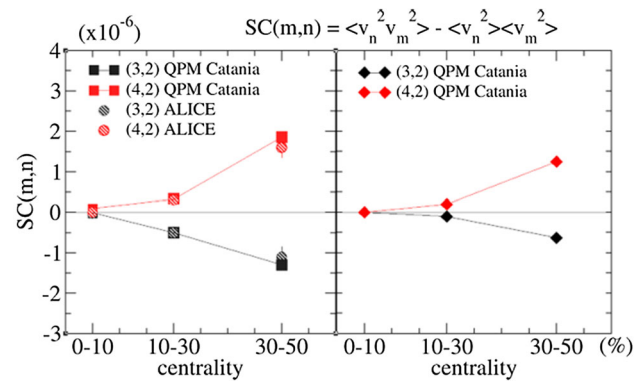
which flow harmonics fluctuate in magnitude event-by-event, and it is defined as follows, starting from the 4-particle correlation:

$$
\begin{aligned}
SC(m&, n) \\
&= \langle\langle\cos(m\phi_1 + n\phi_2 - m\phi_3 - n\phi_4)\rangle\rangle \\
&\quad - \langle\langle\cos(m\phi_1 - m\phi_2)\rangle\rangle\langle\langle\cos(n\phi_1 - n\phi_2)\rangle\rangle = \\
&= \langle v_n^2 v_m^2\rangle - \langle v_n^2\rangle\langle v_m^2\rangle
\end{aligned}
\tag{15}
$$

where the ϕ_i are the particle azimuthal angles, while the double averaging is a mean over all particles and over all events for a given centrality class [67]. Notice that for fixed values of v_n and v_m over all events, the symmetric cumulant as defined in Eq. 15, is zero. We can get this result not only when v_n and v_m are fixed for all events, but also when event-by-event fluctuations of v_n and v_m are uncorrelated. Therefore, the symmetric cumulant is non-zero only if the event-by-event fluctuations of v_n and v_m are correlated.

In Fig. 6, $SC(4, 2)$ (red line) and $SC(3, 2)$ (black line) are shown for $PbPb$ collisions at $\sqrt{s_{NN}} = 5.02$ TeV with $|\eta| < 0.8$ and $0.5 < p_T < 5.0$ GeV as a function of centrality. In the left panel we show the $SC(m, n)$ for charged particles that we compare with the ALICE experimental data [68], predictions for D mesons are shown in the right panel. The results for charged particles are in good agreement with the experimental measurements by ALICE Collaboration. The $SC(4, 2)$ is positive, indicating that for a given centrality interval, events with larger v_2 on average have larger v_4. On the other hand, the $SC(3, 2)$ is negative indicating an anti-correlation between v_2 and v_3 at fixed centrality. This confirm exactly what was observed within the event-shape selected v_n-v_m correlations. As shown in the right panel we predict a weaker but similar behaviour with the centrality for the symmetric cumulant correlator $SC(m, n)$ for D mesons anisotropic flows. For both cases we observe that $SC(4, 2)$ and $SC(3, 2)$ decrease considerably in magnitude from periph-
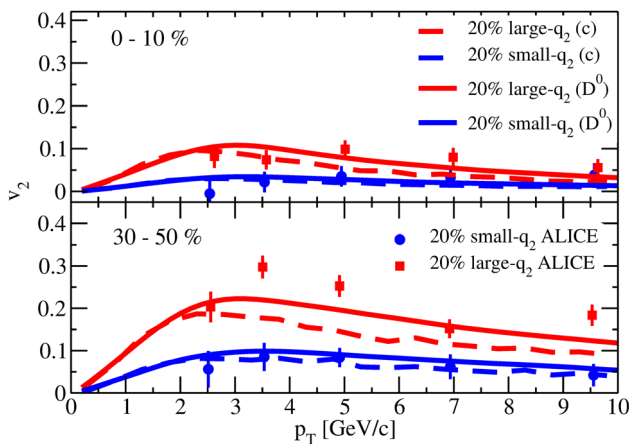
Fig. 7 Elliptic flow v_2 at mid-rapidity for D mesons as a function of p_T in the 20% large-q_2 and 20% small-q_2 events for the centrality classes 0–10% (upper panel) and 30–50% (lower panel) for $PbPb$ collisions at 5.02 TeV. Dashed lines refer to charm quarks v_2 while solid lines refer to D mesons v_2. The experimental data are taken from ALICE measurements [56]
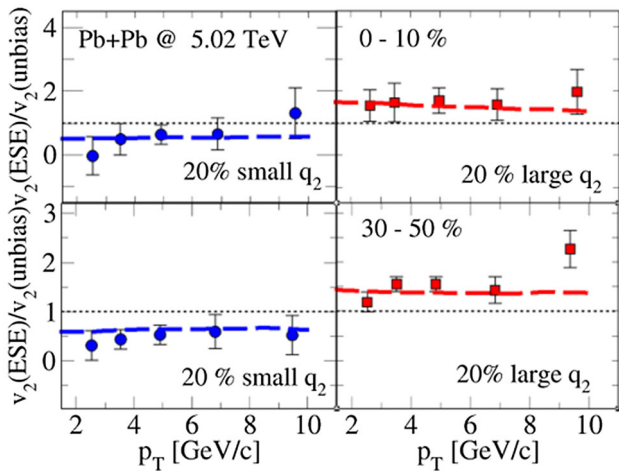
Fig. 8 Ratio of the average D meson v_2 coefficients measured in the 20% large-q_2 (right panel) and 20% small-q_2 (left panel) events with respect to that of the unbiased sample as a function of p_T. These calculation are for for $PbPb$ collisions at 5.02 TeV for two centralities 0–10% (upper panels) and 30–50% (lower panels). The experimental data are taken from ALICE measurements [56]

eral to central events. This large decrease does not imply that the correlations between these harmonics becomes negligible for centrality class smaller then (0–10)%. This decreasing in the magnitude of the correlation occurs since the $SC \sim v_n^4$ and for very central events the v_n (especially v_2) become quite small.

In Fig. 7 we show the results for the D mesons v_2 at mid-rapidity for two centralities and for different q_2 selections: 20% large-q_2 (red solid and dashed lines) and 20% small-q_2 (blue solid and dashed lines) events. As shown in Fig. 7, the v_2 of 20% large-q_2 (red solid line) events is quite larger than the v_2 of 20% small-q_2 events (blue solid line)

for most central 0–10% and semi-peripheral 30–50% centrality classes. This result suggests that the selection in q_2 distinguish between the initial eccentricities, large (small) q_2 means large (small) eccentricity, that consequently develop in large or small transverse flow translated into the final azimuthal anisotropy in momentum space for both bulk and D-meson. This difference increases with the collision centrality. Our results are compared to the ALICE measurements [56], where the good agreement shows that our model can essentially capture the strong coupling between the bulk medium and heavy quark. Finally, in Fig. 8 we show the ratio as a function of the transverse momentum between the D meson v_2 in events characterized by large or small q_2 divided by the v_2 in unbiased events. We find, for these ratios, a difference of about 50% between the q_2-selected and the unbiased events in both centrality class, with no dependence on the transverse momentum, this behaviour might suggest that the ESE selection is related to a global property of the events.

5 Conclusion

In this paper we have studied the propagation of charm quarks in the quark-gluon plasma (QGP) by means of an event-by-event transport approach. In particular we have solved the relativistic Boltzmann transport equation with an event-by-event fluctuating initial condition which allow us to access the study of high order anisotropic flow coefficients v_n for charmed mesons. We have studied the D meson v_n at LHC energies in different centrality class selection. In particular, we have evaluated for the first time the heavy flavor $v_n - v_m$ correlations with the event-shape engineering (ESE) technique consisting in selecting events in the same centrality class but characterized by different average elliptic anisotropy. With our approach we have a good agreement with the available experimental data from ALICE Collaborations for the bulk. Furthermore, we have provided predictions for charmed hadrons $v_n - v_m$ correlations and we predict a weaker but similar correlations behaviour respect to the light flavours reflected in a smaller symmetric cumulant correlator $SC(m, n)$ for D mesons. Like for the light flavor we observe that $SC(4, 2)$ is positive, indicating that for a given centrality interval, events with larger v_2 on average have larger v_4 while the $SC(3, 2)$ is negative indicating an anti-correlation between v_2 and v_3 at fixed centrality. For both cases we observe that $SC(4, 2)$ and $SC(3, 2)$ decrease from peripheral to central events. Finally, we have found that the selection based on the event-shape leads to a visible effect on the final particle elliptic flow. We have shown that the v_2 of 20% large-q_2 events is larger than the v_2 of 20% small-q_2 events for both most central 0–10% and semi-peripheral 30–50% centrality class, suggesting a correlation between the D-meson azimuthal anisotropy and the collective expansion

of the bulk matter. We notice that the sensitivity with the event-shape selection increase with the collision centrality. Our results are in good agreement with the experimental data from the ALICE coll. [56].

Data Availability Statement This manuscript has no associated data or the data will not be deposited. [Authors' comment: This is a theoretical paper and there is no data deposited. The data can be provided when asked.]

Funded by SCOAP³. SCOAP³ supports the goals of the International Year of Basic Sciences for Sustainable Development.

References

1. B.I. Abelev et al., Phys. Rev. Lett. **98**(2007). https://doi.org/10.1103/PhysRevLett.98.192301. [Erratum: Phys. Rev. Lett. 106, 159902 (2011)]
2. S.S. Adler et al., Phys. Rev. Lett. **96**, 032301 (2006). https://doi.org/10.1103/PhysRevLett.96.032301
3. J. Adam et al., JHEP **03**, 081 (2016). https://doi.org/10.1007/JHEP03(2016)081
4. A. Adare et al., Phys. Rev. Lett. **98**, 172301 (2007). https://doi.org/10.1103/PhysRevLett.98.172301
5. B.B. Abelev et al., Phys. Rev. C **90**(3), 034904 (2014). https://doi.org/10.1103/PhysRevC.90.034904
6. H. van Hees, V. Greco, R. Rapp, Phys. Rev. C **73**, 034913 (2006). https://doi.org/10.1103/PhysRevC.73.034913
7. H. van Hees, M. Mannarelli, V. Greco, R. Rapp, Phys. Rev. Lett. **100**, 192301 (2008). https://doi.org/10.1103/PhysRevLett.100.192301
8. P.B. Gossiaux, J. Aichelin, Phys. Rev. C **78**, 014904 (2008). https://doi.org/10.1103/PhysRevC.78.014904
9. S.K. Das, J.E. Alam, P. Mohanty, Phys. Rev. C **80**, 054916 (2009). https://doi.org/10.1103/PhysRevC.80.054916
10. W.M. Alberico, A. Beraudo, A. De Pace, A. Molinari, M. Monteno, M. Nardi, F. Prino, Eur. Phys. J. C **71**, 1666 (2011). https://doi.org/10.1140/epjc/s10052-011-1666-6
11. J. Uphoff, O. Fochler, Z. Xu, C. Greiner, Phys. Lett. B **717**, 430 (2012). https://doi.org/10.1016/j.physletb.2012.09.069
12. T. Lang, H. van Hees, J. Steinheimer, G. Inghirami, M. Bleicher, Phys. Rev. C **93**(1), 014901 (2016). https://doi.org/10.1103/PhysRevC.93.014901
13. T. Song, H. Berrehrah, D. Cabrera, J.M. Torres-Rincon, L. Tolos, W. Cassing, E. Bratkovskaya, Phys. Rev. C **92**(1), 014910 (2015). https://doi.org/10.1103/PhysRevC.92.014910
14. T. Song, H. Berrehrah, D. Cabrera, W. Cassing, E. Bratkovskaya, Phys. Rev. C **93**(3), 034906 (2016). https://doi.org/10.1103/PhysRevC.93.034906
15. S.K. Das, F. Scardina, S. Plumari, V. Greco, Phys. Rev. C **90**, 044901 (2014). https://doi.org/10.1103/PhysRevC.90.044901
16. S. Cao, G.Y. Qin, S.A. Bass, Phys. Rev. C **92**(2), 024907 (2015). https://doi.org/10.1103/PhysRevC.92.024907
17. S.K. Das, F. Scardina, S. Plumari, V. Greco, Phys. Lett. B **747**, 260 (2015). https://doi.org/10.1016/j.physletb.2015.06.003
18. S. Cao, T. Luo, G.Y. Qin, X.N. Wang, Phys. Lett. B **777**, 255 (2018). https://doi.org/10.1016/j.physletb.2017.12.023
19. S.K. Das, M. Ruggieri, F. Scardina, S. Plumari, V. Greco, J. Phys. G **44**(9), 095102 (2017). https://doi.org/10.1088/1361-6471/aa815a
20. Y. Sun, G. Coci, S.K. Das, S. Plumari, M. Ruggieri, V. Greco, Phys. Lett. B **798**, 134933 (2019). https://doi.org/10.1016/j.physletb.2019.134933
21. S. Cao et al., Phys. Rev. C **99**(5), 054907 (2019). https://doi.org/10.1103/PhysRevC.99.054907
22. A. Beraudo et al., Nucl. Phys. A **979**, 21 (2018). https://doi.org/10.1016/j.nuclphysa.2018.09.002
23. S. Plumari, V. Minissale, S.K. Das, G. Coci, V. Greco, Eur. Phys. J. C **78**(4), 348 (2018)
24. V. Minissale, S. Plumari, V. Greco, Phys. Lett. B **821**, 136622 (2021). https://doi.org/10.1016/j.physletb.2021.136622
25. M. Nahrgang, J. Aichelin, S. Bass, P.B. Gossiaux, K. Werner, Phys. Rev. C **91**(1), 014904 (2015). https://doi.org/10.1103/PhysRevC.91.014904
26. C.A.G. Prado, J. Noronha-Hostler, R. Katz, A.A.P. Suaide, J. Noronha, M.G. Munhoz, M.R. Cosentino, Phys. Rev. C **96**(6), 064903 (2017). https://doi.org/10.1103/PhysRevC.96.064903
27. A. Beraudo, A. De Pace, M. Monteno, M. Nardi, F. Prino, Eur. Phys. J. C **79**(6), 494 (2019). https://doi.org/10.1140/epjc/s10052-019-6996-9
28. R. Katz, C.A.G. Prado, J. Noronha-Hostler, J. Noronha, A.A.P. Suaide, Phys. Rev. C **102**(2), 024906 (2020). https://doi.org/10.1103/PhysRevC.102.024906
29. S. Plumari, G. Coci, V. Minissale, S.K. Das, Y. Sun, V. Greco, Phys. Lett. B **805**, 135460 (2020). https://doi.org/10.1016/j.physletb.2020.135460
30. J. Schukraft, A. Timmins, S.A. Voloshin, Phys. Lett. B **719**, 394 (2013). https://doi.org/10.1016/j.physletb.2013.01.045
31. J. Adam et al., Phys. Rev. C **93**(3), 034916 (2016). https://doi.org/10.1103/PhysRevC.93.034916
32. S. Acharya et al., JHEP **02**, 150 (2019). https://doi.org/10.1007/JHEP02(2019)150
33. S. Plumari, A. Puglisi, F. Scardina, V. Greco, Phys. Rev. C **86**, 054902 (2012). https://doi.org/10.1103/PhysRevC.86.054902
34. M. Ruggieri, F. Scardina, S. Plumari, V. Greco, Phys. Lett. B **727**, 177 (2013). https://doi.org/10.1016/j.physletb.2013.10.014
35. F. Scardina, M. Colonna, S. Plumari, V. Greco, Phys. Lett. B **724**, 296 (2013). https://doi.org/10.1016/j.physletb.2013.06.034
36. M. Ruggieri, F. Scardina, S. Plumari, V. Greco, Phys. Rev. C **89**(5), 054914 (2014)
37. A. Puglisi, S. Plumari, V. Greco, Phys. Rev. D **90**, 114009 (2014). https://doi.org/10.1103/PhysRevD.90.114009
38. F. Scardina, D. Perricone, S. Plumari, M. Ruggieri, V. Greco, Phys. Rev. C **90**(5), 054904 (2014). https://doi.org/10.1103/PhysRevC.90.054904
39. S. Plumari, G.L. Guardo, V. Greco, J.Y. Ollitrault, Nucl. Phys. A **941**, 87 (2015). https://doi.org/10.1016/j.nuclphysa.2015.06.005
40. S. Plumari, G.L. Guardo, F. Scardina, V. Greco, Phys. Rev. C **92**(5), 054902 (2015). https://doi.org/10.1103/PhysRevC.92.054902

41. F. Scardina, S.K. Das, V. Minissale, S. Plumari, V. Greco, Phys. Rev. C **96**(4), 044905 (2017)
42. S. Plumari, Eur. Phys. J. C **79**(1), 2 (2019). https://doi.org/10.1140/epjc/s10052-018-6510-9
43. Y. Sun, S. Plumari, V. Greco, Eur. Phys. J. C **80**(1), 16 (2020)
44. S. Plumari, A. Puglisi, M. Colonna, F. Scardina, V. Greco, J. Phys. Conf. Ser. **420**, 012029 (2013). https://doi.org/10.1088/1742-6596/420/1/012029
45. S. Borsanyi, G. Endrodi, Z. Fodor, A. Jakovac, S.D. Katz, S. Krieg, C. Ratti, K.K. Szabo, JHEP **11**, 077 (2010)
46. Z. Xu, C. Greiner, Phys. Rev. C **71**, 064901 (2005). https://doi.org/10.1103/PhysRevC.71.064901
47. G. Ferini, M. Colonna, M. Di Toro, V. Greco, Phys. Lett. B **670**, 325 (2009). https://doi.org/10.1016/j.physletb.2008.10.062
48. P. Bozek, W. Broniowski, M. Rybczynski, Phys. Rev. C **94**(1), 014902 (2016). https://doi.org/10.1103/PhysRevC.94.014902
49. J. Xu, J. Liao, M. Gyulassy, JHEP **02**, 169 (2016). https://doi.org/10.1007/JHEP02(2016)169
50. M. Cacciari, S. Frixione, N. Houdeau, M.L. Mangano, P. Nason, G. Ridolfi, JHEP **10**, 137 (2012)
51. C. Peterson, D. Schlatter, I. Schmitt, P.M. Zerwas, Phys. Rev. D **27**, 105 (1983). https://doi.org/10.1103/PhysRevD.27.105
52. G.D. Moore, D. Teaney, Phys. Rev. C **71**, 064904 (2005). https://doi.org/10.1103/PhysRevC.71.064904
53. V. Minissale, F. Scardina, V. Greco, Phys. Rev. C **92**(5), 054904 (2015)
54. S. Chatrchyan et al., JHEP **07**, 076 (2011). https://doi.org/10.1007/JHEP07(2011)076
55. S. Chatrchyan et al., Eur. Phys. J. C **72**, 2012 (2012). https://doi.org/10.1140/epjc/s10052-012-2012-3
56. S. Acharya et al., Phys. Lett. B **813**, 136054 (2021). https://doi.org/10.1016/j.physletb.2020.136054
57. H. Niemi, G.S. Denicol, H. Holopainen, P. Huovinen, Phys. Rev. C **87**(5), 054901 (2013). https://doi.org/10.1103/PhysRevC.87.054901
58. B. Abelev et al., Phys. Lett. B **719**, 18 (2013). https://doi.org/10.1016/j.physletb.2012.12.066
59. S. Acharya et al., JHEP **09**, 108 (2019). https://doi.org/10.1007/JHEP09(2019)108
60. U. Heinz, R. Snellings, Annu. Rev. Nucl. Part. Sci. **63**, 123 (2013). https://doi.org/10.1146/annurev-nucl-102212-170540
61. F.G. Gardim, F. Grassi, M. Luzum, J.Y. Ollitrault, Nucl. Phys. A **904–905**, 503c (2013). https://doi.org/10.1016/j.nuclphysa.2013.02.063
62. S.A. Voloshin, A.M. Poskanzer, R. Snellings, Landolt-Bornstein **23**, 293 (2010). https://doi.org/10.1007/978-3-642-01539-7_10
63. S. Mohapatra, Nucl. Phys. A **956**, 59 (2016). https://doi.org/10.1016/j.nuclphysa.2016.06.003
64. G. Aad et al., Phys. Rev. C **92**(3), 034903 (2015). https://doi.org/10.1103/PhysRevC.92.034903
65. F.G. Gardim, F. Grassi, M. Luzum, J.Y. Ollitrault, Phys. Rev. C **85**, 024908 (2012). https://doi.org/10.1103/PhysRevC.85.024908
66. S. Floerchinger, U.A. Wiedemann, A. Beraudo, L. Del Zanna, G. Inghirami, V. Rolando, Phys. Lett. B **735**, 305–310 (2014). https://doi.org/10.1016/j.physletb.2014.06.049
67. A. Bilandzic, C.H. Christensen, K. Gulbrandsen, A. Hansen, Y. Zhou, Phys. Rev. C **89**(6), 064904 (2014). https://doi.org/10.1103/PhysRevC.89.064904
68. S. Acharya et al., Phys. Lett. B **818**, 136354 (2021). https://doi.org/10.1016/j.physletb.2021.136354